Experimental determination of entropy and exergy in low cycle fatigue

Patrick Ribeiro*, Johann Petit, Laurent Gallimard

Université Paris Nanterre - 50, rue de Sèvres 92410 Ville d'Avray France

Abstract

Recent works in mechanical fatigue consider that a threshold of entropy exists, the fracture fatigue entropy. In this paper, we observe the existence of a threshold of entropy and exergy in low cycle fatigue for a flat Al-2024 measuring the heat generated during a fatigue test. Results are compared considering various hypotheses (1D heat dissipation with convection and radiation considered as complementary parts, and, heat transfer from a fin with convection and radiation as boundary conditions) to an empirical mechanical model known in the literature and deviations between them are discussed.

Keywords: Fracture Fatigue Entropy, Thermography, Exergy

1. Introduction

Fatigue of metallic materials has always been a major concern in the design of mechanical parts and structures submitted to cyclic stresses. Since the seminal work of Wöhler [1], numerous methods and models have been proposed to estimate the fatigue life of a material. They are generally based on quantities such as the number of cycle to failure [2–10], energy dissipation [11–14] or entropy [15–18]. Identification of the model parameters can be done from experimental data obtained by non intrusive testing such as digital image correlation [19, 20], acoustic emission [21–23] or infrared thermal imaging [24–26]. Energy dissipation is largely used to estimate fatigue life. It is mostly related to heat and thus to the variation of temperature in the specimen [27]. Consequently, specimen temperature evolution rises as an

*Corresponding author.
Email address: patrick.ribeiro@parisnanterre.fr (Patrick Ribeiro)

important quantity to assess fatigue life of a material [28–31], as well as heat dissipated during fatigue tests [32, 33] which appears to be an appropriate fatigue damage index [34–36].

In the thermodynamic view, fatigue damage mechanisms are seen as irreversible phenomena, fundamentally related to entropy generation. Classical and statistical entropy-based approaches have been investigated to estimate damage and time to failure [37–41]. Based on the second law, [42] observed that cumulative entropy generation can be seen as a material property and named it fracture fatigue entropy (FFE). In these papers, the experimental tests on low cycle and high cycle fatigue, in which entropy is directly determined from the number of cycles to failure, showed that the FFE is a constant for each material independent of loading type, frequency and amplitude as well as the geometry of the specimen but would depend on stress concentration [43–49]. This concept is actively influencing recent works on fatigue such as reliability [50–52], damage estimations [53–57] and temperature response of the material [58]. Finally, it is worth mentioning that other experimental observations lead to the estimation of the FFE only by using the initial slope of temperature rise [59–62].

To compute the FFE from experimental results, empirical models are used such as the Park and Nelson model. However, this approach does not fully exploit the infrared thermography measurements, where temperature can give information on the energy dissipated during the test. This paper is focused on the experimental estimation of the fracture fatigue entropy (FFE) and the comparison with the FFE obtained from empirical Park and Nelson's model. In the present case, the FFE is determined by temperature field measurements carried out throughout the tests and direct calculation of the entropy according to two different models. After the presentation of the thermomechanical background and the experimental setup, the different models for the estimation of the FFE and exergy of plastic deformation are presented. Then, a discussion about the various results and some perspectives are given.

2. Thermomechanical formulation and experimental setup

2.1. Thermodynamical framework

The two laws of thermodynamics are applied to a specimen submitted to fatigue:

$$\rho\dot{u} = -div\,\dot{Q} + \sigma : D \qquad \rho\dot{s} = -div\left(\frac{\dot{Q}}{T}\right) + \dot{\pi} \tag{1}$$

The second law can be developed as:

$$\rho\dot{s} + \frac{div\,\dot{Q}}{T} - \left(\frac{\dot{Q}}{T^2}\cdot\nabla T\right) = \dot{\pi} \geq 0 \tag{2}$$

where $\dot{\pi}$ is the specific entropy generated flow, produced by the irreversibility of the thermodynamical transformation. Replacing the first principle in the second law, and using the Helmholtz free energy ($\psi = u - Ts$) leads to:

$$\frac{-\rho}{T}\left[\left(\dot{\psi} + s\dot{T}\right)\right] + \frac{\sigma : D}{T} - \left(\frac{\dot{Q}}{T^2}\cdot\nabla T\right) \geq 0 \tag{3}$$

Free energy is considered as a function of multiple state variables (introducing V_k a set of internal variables) [63]:

$$\dot{\psi} = \frac{d\psi}{d\epsilon_e} : \dot{\epsilon}_e + \frac{d\psi}{dT}\dot{T} + \underbrace{\frac{d\psi}{dV_k}}_{A_k}\dot{V}_k \tag{4}$$

To simplify, the small deformation hypothesis can be used in low cycle fatigue ($D = \dot{\epsilon}_e + \dot{\epsilon}_p$). It leads to the expression of the specific entropy generated flow:

$$\dot{\pi} = \frac{\sigma : \dot{\epsilon_p}}{T} + \left(-\frac{A_k\dot{V}_k}{T}\right) + \left(-\frac{\dot{Q}}{T^2}\cdot\nabla T\right) \geq 0 \tag{5}$$

Where:

- $\left[\frac{\sigma : \dot{\epsilon_p}}{T}\right]$ is the specific entropy flux generated by plastic deformation
- $\left[-\frac{A_k\dot{V}_k}{T}\right]$ is the specific entropy flux generated by irreversible deformation mechanisms (strain hardening, phase transformation ...)

- $\left[-\frac{\dot{Q}}{T^2}\cdot\nabla T\right]$ is the specific entropy flux generated by heat conduction

The fracture fatigue entropy [44] or the maximum entropy generated by irreversibility during fatigue is:

$$FFE = \int_0^{t_f} \dot{\pi} dt \tag{6}$$

t_f being the time to failure. In our case, we will concentrate on low cycle fatigue for an Al-2024 specimen. For low hardenable specimen and for high enough test speed, the second and the third terms in equation (5) are generally neglected [63]:

$$\left|\frac{A_k \dot{V}_k}{T}\right| << \left|\frac{\sigma : \dot{\epsilon_p}}{T}\right| \qquad \left|\frac{\dot{Q}}{T^2}\cdot\nabla T\right| << \left|\frac{\sigma : \dot{\epsilon_p}}{T}\right| \tag{7}$$

The flux of entropy produced reduces in this case to:

$$\dot{\pi} = \frac{\sigma : \dot{\epsilon_p}}{T} \geq 0. \tag{8}$$

2.2. Experimental procedure and hypotheses

Experimental tests are done on an Al-2024 specimen using an INSTRON 8501 device allowing repeated traction tests ($R = 0$) for different loading stress comprised between 390 and 465 MPa and with loading frequencies of 5 and 10 Hz. An infrared camera FLIR A325sc is used to measure surface temperature (working wavelength 7.5-13 μm). The different configurations are summarised in Table.1 and the material properties are presented in Table.2.

The main hypotheses used in this study are:

- An unidirectional diffusion of heat, flowing only in the specimen length direction since jaws of the fatigue machine act as temperature sinks. We can verify this assumption experimentally, or using the Biot number (Bi~ $10^{-5} << 1$).
- The plastic deformation work is completely converted into heat.
- The plastic deformation work is assumed homogeneous implying the source term in the heat equation to be space independent.

Frequency $[Hz]$	Test Number $[-]$	Stress $[MPa]$	Emissivity $[-]$	Dimensions $[mm]$
5	N°1 - N°2	430	0.95	57×12.5×2
	N°3 - N°4	450		
	N°5 - N°6	470		
10	N°7	410		
	N°8	430		
	N°9	450		
	N°10	470		

Table 1: Different configurations of tests performed on Al-2024 specimens

Density $[kg.m^{-3}]$	Thermal Conductivity $[W.m^{-1}.K^{-1}]$	Heat Capacity $[J.kg^{-1}.K^{-1}]$	YTS $[MPa]$	UTS $[MPa]$	Young Modulus $[GPa]$
2780	121	875	345	480	73.1

Table 2: Properties of the Al-2024

3. FFE calculation

As shown in section 2, the calculation of the FFE requires the measurement of temperature and plastic deformation work. In the literature, the work of plastic deformation is estimated by empirical models such as the Morrow equation or the Park and Nelson model [42, 48]. In this work, an estimate of this entropy is obtained by only using experimental results from the temperature measurements. In subsection 3.1, the Park and Nelson empirical model found in the literature is introduced, then, in subsection 3.2, FFE is estimated from infrared thermography.

3.1. FFE calculation with an empirical mechanical model

The empirical model used to estimate the entropy generated during fatigue is the Park and Nelson model [8] which relates the cyclic deformation work to the number of cycles endured by the material:

$$W_T = W_p + W_e = AN_f^{\alpha} + BN_f^{\beta} \tag{9}$$

$$A = 2^{2+b+c}\sigma'_f\epsilon'_f\left(\frac{c-b}{c+b}\right) \qquad \alpha = b + c \qquad B = \frac{2^{2b+1}\left(1+\nu\right)\sigma'^{\,2}_f}{3E_y} \qquad \beta = 2b \tag{10}$$

Since the elastic part of deformation does not appear in the entropy generation, we only keep the plastic deformation rate which is estimated by:

$$\sigma : \dot{\epsilon}_p = f \times A N_f^{\alpha} \tag{11}$$

The fatigue parameters $(\sigma'_f, \epsilon'_f, b, c)$ are estimated using two common laws from literature, the Uniform Material Law (UML) from [64] and the Median Method (MM) from [65]. For aluminum alloys, the parameters are given by:

$$\sigma'_f = 1.67\,UTS \qquad \epsilon'_f = 0.35 \qquad b = -0.095 \qquad c = -0.69 \qquad \textbf{UML} \tag{12}$$

$$\sigma'_f = 1.9\,UTS \qquad \epsilon'_f = 0.28 \qquad b = -0.11 \qquad c = -0.66 \qquad \textbf{MM} \tag{13}$$

Note that the coefficient of variation of the fatigue parameters can be large and thus lead to inaccuracy in fatigue life estimation [65, 66].

To take into account the mean stress (since $R = 0$), we can use the Dowling formulation [67, 68], leading to the prefactor:

$$m = \left(\frac{1 - R}{2}\right)^{c/2b} \tag{14}$$

with R, the loading ratio.

The entropy generated is finally:

$$FFE_{PN} = \int_0^{t_f} \frac{m \times f \times A N_f^{\alpha}}{T}\, dt \tag{15}$$

where FFE_{PN} refers to the estimation using Park and Nelson's model.

3.2. FFE calculation using thermography

3.2.1. Estimation without convection and radiative parts

Using energy conservation leads directly to the estimation of the fracture fatigue entropy by heat dissipation (HD):

$$FFE_{HD} = \int_0^{t_f} \left(\frac{\rho C \dot{T} + div\, \dot{Q}}{T}\right) dt \tag{16}$$

Note that thermoelastic and thermoplastic couplings are not taken into account, indeed, thermoelasticity vanishes on one cycle and thermoplastic coupling is negligible when the mechanical behaviour varies little with temperature.

The thermal evolution of the material in the present case exhibits two distinct phases. At the beginning of the fatigue test (non stationary phase), plastic deformation is predominant implying a rapid increase in temperature (see figure 1). Then, the work hardening of the material can accommodate the deformation and the temperature is observed to decrease until the second phase. This latter (steady state) shows a stabilisation in the thermal behaviour of the material ; the macroscopic mechanical behaviour has turned elastic nevertheless plasticity remains, as shown in figure 1 by the positive temperature difference with the outside. During this phase, there is an equilibrium between heat production by plastic strain mechanisms and heat losses with exterior.

(a) Heat accumulation estimation:
Heat accumulation ($\rho C\dot{T}$) is evaluated by the use of a spatial mean temperature solely dependent on time (considering a homogeneous mechanical deformation). A piece-wise linear spatial mean temperature evolution (T_m) is used to characterise the energy accumulation:

$$T_m(t) = a_i t + b_i \qquad \left(\frac{dT_m}{dt}\right)_i = a_i \qquad t \in [t_i, t_{i+1}] \subset [0, t_f] \tag{17}$$

a_i : represents the temperature variation in time obtained by linear fit in the temporal range $[t_i, t_{i+1}]$, this range being included in the entire temporal range $[0, t_f]$, b_i a parameter obtained by fit for continuity, and with t_f being the time of duration of the test.

The power and entropy accumulated in the sample are calculated using:

$$P_{ac} = \rho C\dot{T} \approx \rho C\dot{T}_m \tag{18}$$

$$FFE_{ac} = \int_0^{t_f} \frac{\rho C\dot{T}}{T} dt \approx \int_0^{t_f} \frac{P_{ac}}{T_m(t)} dt = \rho C \sum_i \ln\left(\frac{a_i t_{i+1} + b_i}{a_i t_i + b_i}\right) \tag{19}$$

For the sake of brevity, the integral form of the different FFE expressions will be kept in the following equations.

(b) Heat conduction estimation:
For the heat conduction estimation, considering that heat sources coming from the mechanical deformation are spatially uniform allows the use of a parabolic fit for the temperature profile along the specimen

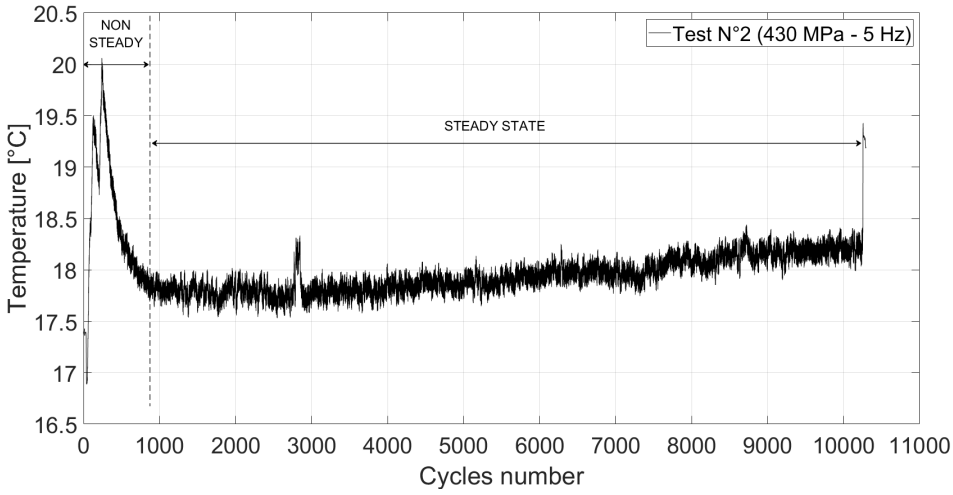

Figure 1: Temperature evolution for the Test N°2 (430 MPa - 5Hz) where two different thermal regimes can be observed

(see figure 2). The estimation of the three fit parameters enables the calculation of the thermal conduction power through the material (1D hypothesis), where the spatial temperature profile is fitted at many time steps to deal with time effects:

$$T(y) = a_y y^2 + b_y y + c_y \qquad P_{co}(t) = -k\frac{d^2T}{dy^2}(t) = -2ka_y(t) \tag{20}$$

$$FFE_{co} = \int_0^{t_f} \frac{div\,\dot{Q}(t)}{T}dt \approx \int_0^{t_f} \frac{P_{co}(t)}{T_m(t)}dt = \int_0^{t_f} \frac{-2ka_y(t)}{T_m(t)}dt \tag{21}$$

The overall generated entropy is then estimated as:

$$FFE_{HD} = FFE_{co} + FFE_{ac} \approx \int_0^{t_f} \frac{-2ka_y(t)}{T_m(t)}dt + \int_0^{t_f} \rho C\left(\frac{\dot{T}_m(t)}{T_m(t)}\right)dt \tag{22}$$

3.2.2. Estimation including convection and radiation

(a) Considering convection and radiation as complementary parts

One can improve the former estimation taking into account the convective and radiative parts [12, 32]. The estimation of fatigue fracture

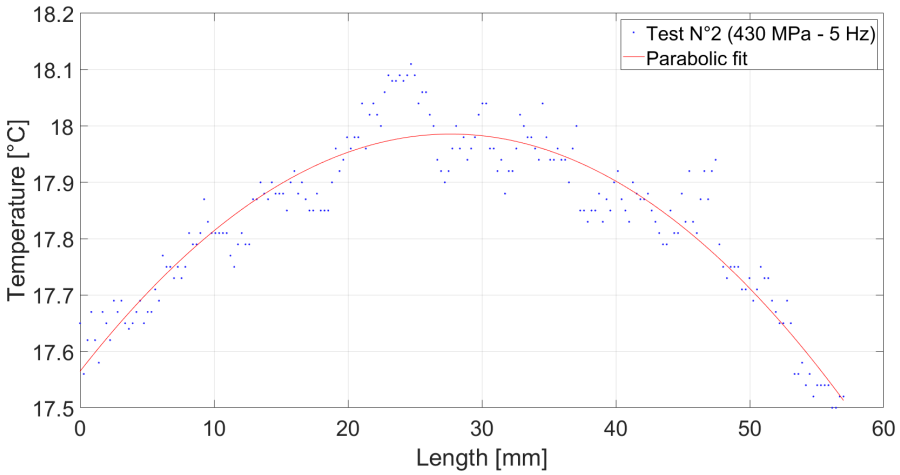

Figure 2: Parabolic fit and measured temperature along the length (centerline) of the specimen at $t \approx 322s$ (Test N°2)

entropy is possible considering these two parts as complementary parts adding their contribution to equation (22). Thereby the total entropy generated during the fatigue tests can be obtained from Thermal Balance:

$$FFE_{TB} = \int_0^{t_f} \left(\frac{\rho C \dot{T} + P_{co} + P_{conv} + P_{rad}}{T} \right) dt \tag{23}$$

The specific convective and radiative dissipated power is estimated by:

$$(P_{conv} + P_{rad}) = h_G \frac{S_{conv}}{V_{spe}} (T_m(t) - T_0) \qquad h_G = h_{conv} + h_{rad} \tag{24}$$

With:

$S_{conv} = 2 \times L \times l + 2 \times L \times e_p$ is the exchange surface

$V_{spe} = l \times L \times e_p$ is the specimen volume

L,l,e_p are the length, width and thickness respectively

The global heat transfer coefficient h_G is the sum of a convective part h_{conv} and a radiative part h_{rad}. The heat convection coefficient is estimated using several correlations from the literature (see Appendix A for more details). For the radiation, a Taylor expansion is used near

the environment temperature T_0 (linearization of the Stefan-Boltzmann law), which is near 288.15K:

$$T_m^4(t) = T_0^4 + 4T_0^3\left(T_m(t) - T_0\right) \qquad h_{rad} = 4\varepsilon\varsigma T_0^3 \approx 5.3\, W m^{-2} K^{-1} \quad (25)$$

With ϵ the emissivity (taken as 0.95) and $\varsigma = 5.67 \times 10^{-8} W m^{-2} K^{-4}$, the Stefan-Boltzmann constant. More details on emissivity uncertainties are discussed in Appendix B. The generated entropy from convection and radiation is then estimated by:

$$FFE_{conv} + FFE_{rad} \approx \int_0^{t_f} \frac{\left[h_G \frac{S_{conv}}{V_{spe}}\left(T_m(t) - T_0\right)\right]}{T_m(t)} dt \quad (26)$$

Finally including all the contributions leads to:

$$FFE_{TB} = FFE_{co} + FFE_{ac} + FFE_{conv} + FFE_{rad} \quad (27)$$

$$FFE_{TB} \approx \int_0^{t_f} \frac{-2ka_y(t)}{T_m(t)} dt + \int_0^{t_f} \rho C \left(\frac{\dot{T}_m(t)}{T_m(t)}\right) dt + \int_0^{t_f} \frac{\left[h_G \frac{S_{conv}}{V_{spe}}\left(T_m(t) - T_0\right)\right]}{T_m(t)} dt \quad (28)$$

(b) Considering convection and radiation from the boundary conditions
Another model from the literature permits the estimation of intrinsic dissipation d_1 in the material [33, 69–72]. Based on the heat conduction and assuming an uniform temperature across the thickness and the width (with Robin boundary conditions) leads to a thermal fin like equation (1D hypothesis):

$$\rho C \dot{\theta}_T + \rho C \frac{\theta_T}{\tau} - k \frac{\partial^2 \theta_T}{\partial y^2} = d_1 \qquad \theta_T = \left(T_m - T_0\right) \quad (29)$$

$$\tau = \frac{\rho C e_p l}{2h_G(e_p + l)} \qquad h_G = h_{conv} + h_{rad} \quad (30)$$

The entropy is thus directly estimated through:

$$FFE_{d1} = \int_0^{t_f} \frac{d_1}{T} dt \quad (31)$$

The same procedure as previously is used to evaluate heat accumulation. The estimation of d_1, also assumed uniform along the specimen, can be obtained by fitting the temperature profile along the specimen gauge length (see figure 3) according to the following expression:

$$\theta_T = P_1 \exp^{y\sqrt{\frac{\rho C}{k\tau}}} + P_2 \exp^{-y\sqrt{\frac{\rho C}{k\tau}}} + \frac{\tau d_1}{\rho C} \tag{32}$$

P_1 and P_2 being two coefficients to be identified.

To take into account time evolution, we can consider a constant d_1 on the temporal range $[t_i, t_{i+1}]$, the dissipated power is evaluated as (for Thermal Fin):

$$P_{TF} = \overline{d_1} = \left(\frac{1}{t_f}\right) \int_0^{t_f} d_1(t)dt \approx \left(\frac{1}{t_f}\right) \sum_n d_1(t_n)(t_{n+1} - t_n) \tag{33}$$

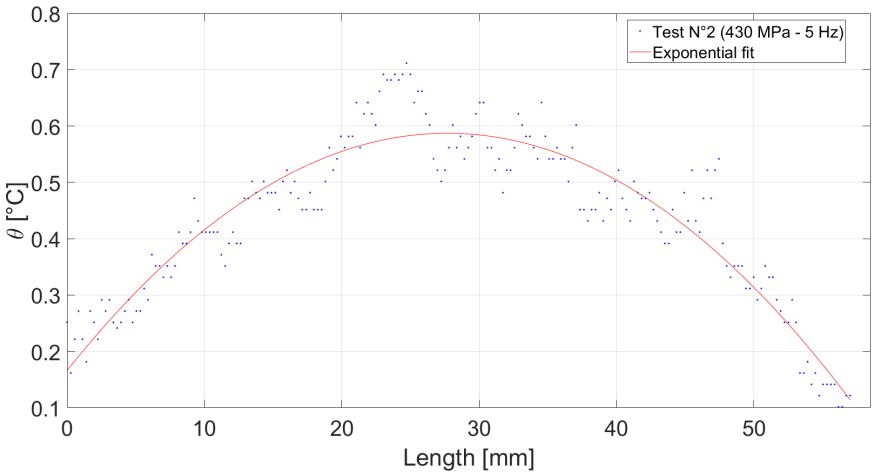

Figure 3: Exponential fit and measured temperature along the length (centerline) of the specimen at $t \approx 322s$ (Test N°2)

And the generated entropy is given by:

$$FFE_{TF} \approx \int_0^{t_f} \rho C \left(\frac{\dot{T}_m(t)}{T_m(t)}\right) dt + \int_0^{t_f} \frac{d_1(t)}{T_m(t)} dt \tag{34}$$

3.2.3. FFE time evolution

The temporal evolution of the fracture fatigue entropy can be analysed using an interval time-based integration. The mean time rate of the fatigue entropy $F\dot{F}E_j$ on each interval $[t_j, t_{j+1}]$ is given by:

$$F\dot{F}E_j \approx \left(\frac{1}{t_{j+1} - t_j}\right) \int_{t_j}^{t_{j+1}} \frac{P(t)}{T_m(t)} dt \tag{35}$$

P being the power corresponding to the quantity under study (P_{ac},P_{co},P_{conv},P_{rad} or P_{d1}).

Another quantity to investigate temporal evolution is the cumulative entropy generation in the temporal range $[0, t_j]$ with $t_j \leq t_f$, which is calculated using:

$$FFE_c \approx \int_0^{t_j} \frac{P(t)}{T_m(t)} dt \tag{36}$$

This quantity is very important since it permits to verify the second law of thermodynamics at each time, i.e. $FFE_{TB} \geq 0$ and $FFE_{TF} \geq 0$.

Besides entropy, another thermodynamical quantity called exergy can be used to complete the mechanical analysis.

4. Exergy calculation

The thermodynamical study so far is based on the two classical principles. Thus, a new thermodynamical quantity is necessary if we want to extend the thermodynamical study of fatigue.

The notion of quality is important in the field of thermodynamics, indeed, from the point of view of the first principle, an energetical hierarchy does not exist. However, the second principle allows to distinguish the different energies in particular the non equivalence heat-work. To do so, it is possible to create a thermodynamical potential taking into account the environmental effects and allowing the conversion of any energy into an equivalent quantity, a mechanical equivalent potential called exergy (see [73–75] for details on the history of this quantity), defined as the maximum useful work recoverable from a system in contact with the environment or as a distance from equilibrium.

Exergy in fatigue can be expressed as a linear combination of the first and second principle (considering negligible the work exerted by the room

pressure on the material) :

$$\rho\dot{x} = \rho\left(\dot{u} - T_0\dot{s}\right) \tag{37}$$

Developing each terms leads to [76]:

$$\rho\dot{x} = \underbrace{-div\,\dot{Q}\left(1 - \frac{T_0}{T}\right)}_{\dot{x}_q} + \underbrace{\sigma : \dot{\epsilon_p}\left(1 - \frac{T_0}{T}\right)}_{\dot{x}_p} + \underbrace{\sigma : \dot{\epsilon_e}}_{\dot{x}_e} - \underbrace{\left(-\frac{T_0}{T}A_k\dot{V}_k\right)}_{\dot{an}_k} \tag{38}$$

$\dot{x}_e$: Specific exergy flow associated to elastic deformation

$\dot{x}_q$: Specific exergy flow associated to heat transfer

$\dot{x}_p$: Specific exergy flow associated to plastic deformation

$\dot{an}_k$: Specific anergy flow associated to internal variables

$C_a = \left(1 - \frac{T_0}{T}\right)$: Carnot Factor

This equation highlights that the energy of plastic deformation has a lower quality than pure mechanical work (the Carnot Factor acts as the quality factor) making the deformation as a particular mechanical phenomenon. In other terms, if a machine could receive energy accumulated during a material's fatigue, it would get more energy (exergy) from a material's fatigue at higher temperature than a material's fatigue at lower temperature. We will thus concentrate on the exergy of plastic deformation. The plastic exergy generated can be expressed as a function of the FFE:

$$x_p = \int_0^{t_f} \dot{x}_p dt \approx \int_0^{t_f} \sigma : \dot{\epsilon_p}\left(1 - \frac{T_0}{T_m(t)}\right) dt \tag{39}$$

The advantage of this quantity is to take into account the effect of the environment temperature on the fatigue irreversibility. Furthermore, for time studies, this quantity can also be treated as the FFE according to equation (35) and equation (36) to get the mean time derivative and the cumulative plastic exergy.

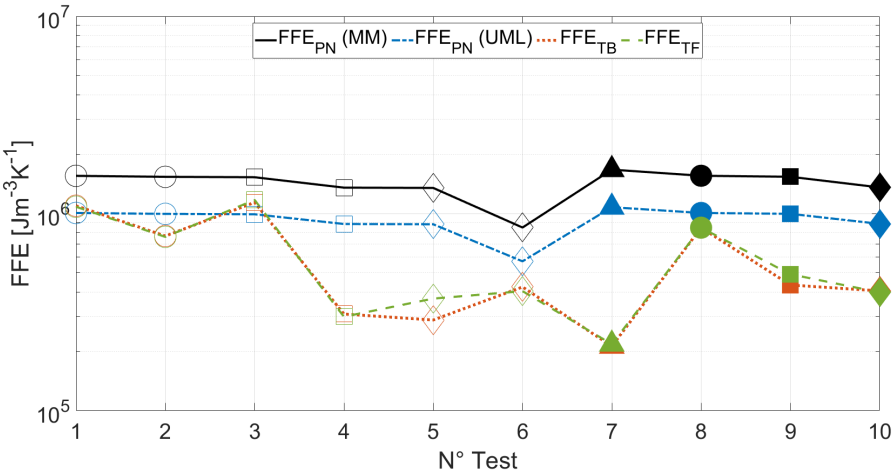

Figure 4: FFE comparison between experimental methods (TB and TF) and empirical model (PN) - Loads : △ : 410 MPa - ○ : 430 MPa - □ : 450 MPa - ◇ : 470 MPa ; Frequencies : Unfilled markers : 5 Hz - Filled markers : 10 Hz

5. Results and discussion

Two approaches have been compared to estimate the fracture fatigue entropy of a material. The first approach uses a classical empirical mechanical model (Park and Nelson) and fatigue parameters from literature (Uniform Material Law and Median Method) with a particular prefactor taking into account the mean stress ($R = 0$). The second one is based on the experimental temperature measurement by thermography to estimate the heat flowing in the material. The first estimation (parabolic fit) of the FFE can be refined taking into account convective and radiative parts as complementary parts. The second estimation (exponential fit) takes convective and radiative parts as boundary conditions. Finally, the exergy of plastic deformation which traduces the thermodynamic quality of the mechanical deformation has also been investigated.

5.1. Fracture fatigue entropy

The existence of a threshold, i.e. a constant value of the fracture fatigue entropy for the Al-2024 is here observed experimentally in an uncertainty range of less than one decade and appears to be an intrinsic parameter of the material, independent of the load and potentially of the frequency, but the limited experimental data on frequency does not allow to conclude with

certainty. This observation supports the work of [42, 44] on the fracture fatigue entropy. Indeed, the experimental methods used to obtain the fracture fatigue entropy value (FFE_{TB} and FFE_{TF}) provide similar results validating each other. In addition, the Park and Nelson empirical model (corrected with the mean stress prefactor) is found to be in accordance with the experimental results, in particular with fatigue parameters from the Uniform Material Law (see figure 4).

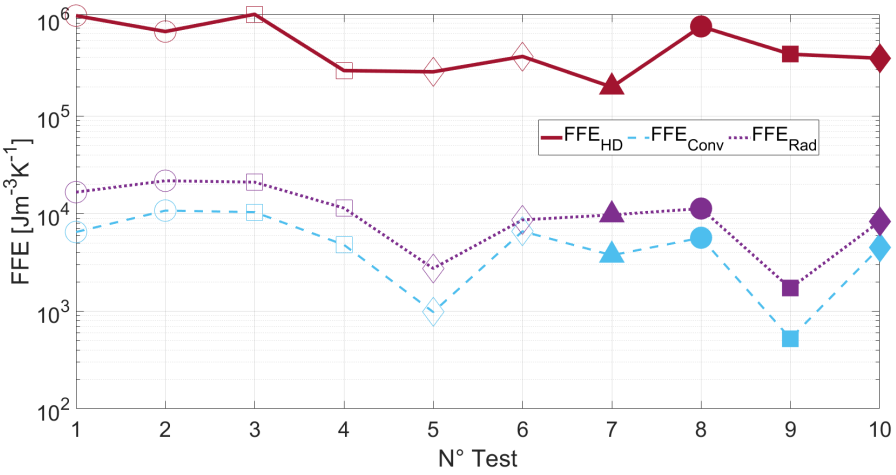

Figure 5: FFE comparison between heat dissipation (TB) and convective (conv) and radiative (rad) parts - Loads : △ : 410 MPa - ○ : 430 MPa - □ : 450 MPa - ◇ : 470 MPa ; Frequencies : Unfilled markers : 5 Hz - Filled markers : 10 Hz

From these tests, it can be seen that the components of convection and radiation are negligible compared to pure conduction (the ratio of $FFE_{conv} + FFE_{rad}$ to FFE_{TB} is on average equal to 3.13%, see figure 5).

The results presented in figure 6 show an important part of the FFE created during the first phase (non stationary phase) of the fatigue test i.e. created by the initial work hardening ($FFE_{ac,j} + FFE_{co,j}$ or $FFE_{ac,j} + FFE_{d1,j}$). After this phase, strain is converted into heat almost steadily, leading to stable fatigue entropy generation ($FFE_{co,j}$ or $FFE_{d1,j}$). The convection and radiation parts appear marginal during the fatigue test. The quantity FFE_c shows two tendencies, entropy accumulates very quickly (fast burst) in the unsteady phase and then tends to stabilise (seems to be linear) in the stationary phase. Moreover, the results show positive $FFE_{TB,c}$ and positive $FFE_{TF,c}$ respecting the second law of thermodynamics.

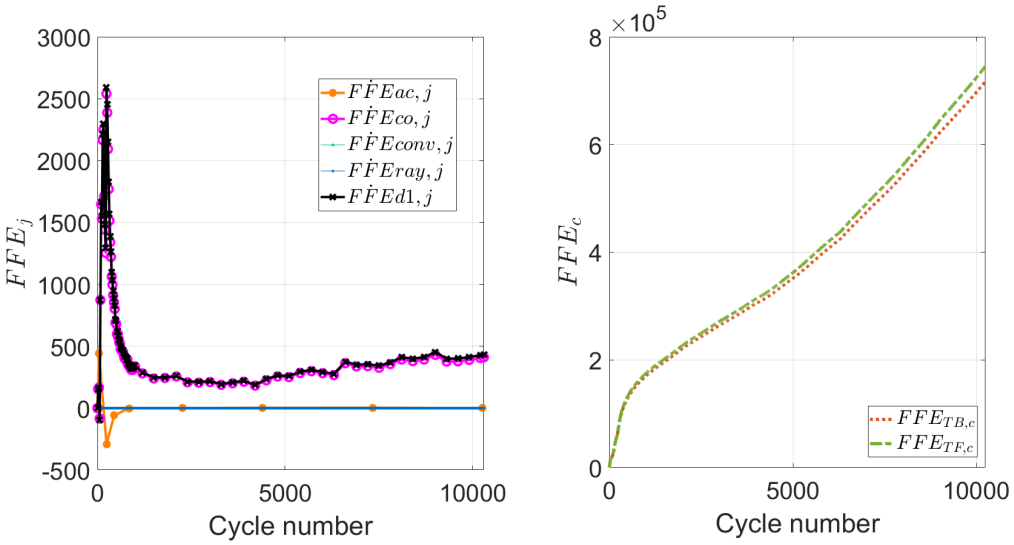

Figure 6: Time rate of the generated fatigue entropy $F\dot{F}E_j$ and cumulative generated fatigue entropy FFE_c calculated for the test N°2 (430 MPa - 5Hz) as a function of the number of cycles

5.2. Exergy of plastic deformation

The results of the exergy of plastic deformation are plotted in figure 7. These results consolidate the FFE results where a threshold of exergy of plastic deformation seems to exist. The advantage of the exergy of plastic deformation is that it takes into account the influence of the environment on the irreversibility of the thermodynamical system and compares different tests under various environmental conditions. Even if, there is no significant difference between the evolution of the FFE and x_p, it can be seen that taking into account the environment temperature acts as a normalisation.

Like the FFE_j, estimating a ${x_p}^j$ between $[t_j, t_{j+1}]$ shows that the material is highly affected at the beginning of the lifetime of the material. Using the exergy of plastic deformation enables to highlight the thermodynamical degradation of the material. In proportion along the test, more exergy is developed during the non stationary phase than generated entropy. For a stress ratio $R = 0$, the first rather short non stationary phase appears to be quite damaging, especially when the damage indicator is exergy (see figure 8 versus figure 6).

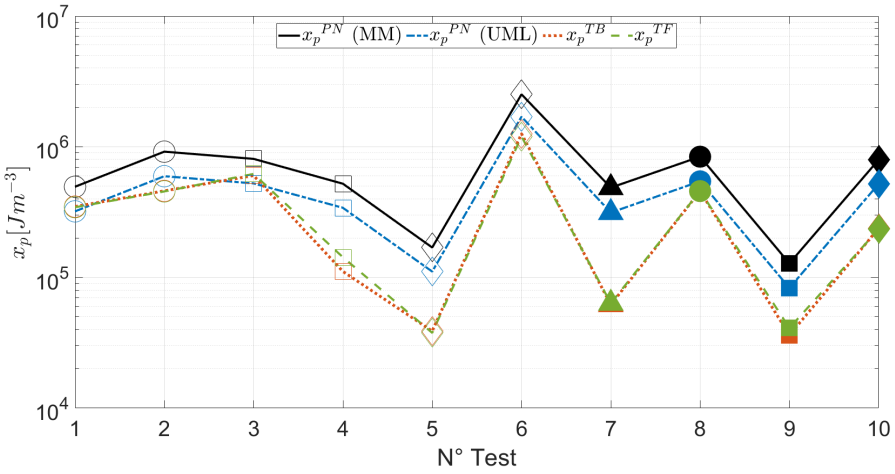

Figure 7: Exergy of plastic deformation dissipated during fatigue for each test, obtained by two experimental methods (TB and TF) and the empirical model (PN) - Loads : △ : 410 MPa - ○ : 430 MPa - □ : 450 MPa - ◇ : 470 MPa ; Frequencies : Unfilled markers : 5 Hz - Filled markers : 10 Hz

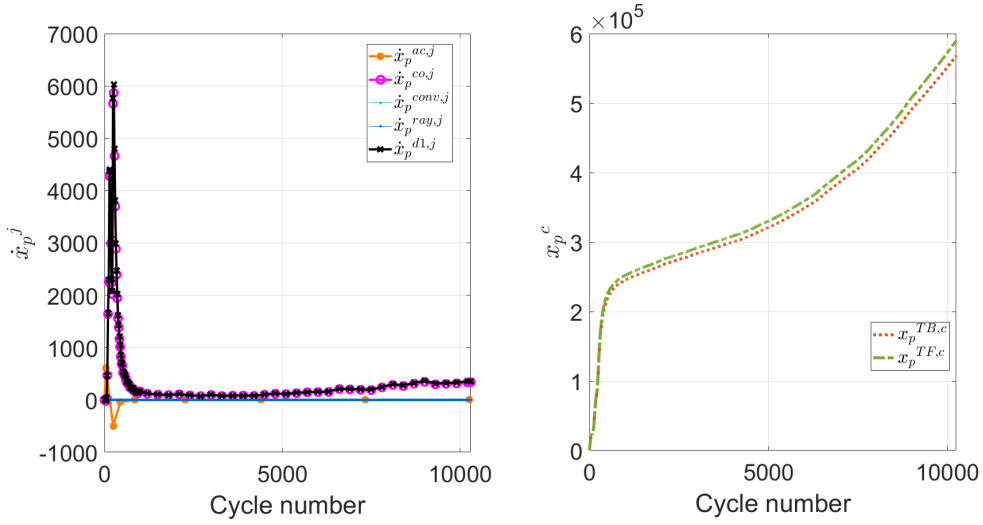

Figure 8: Time rate of the exergy $\dot{x}_p^j$ and cumulative exergy ${x_p}^c$ for the test N°2 (430 MPa - 5 Hz) as a function of the number of cycles

6. Conclusion and perspectives

In this paper, low cycle fatigue of an aluminum alloy Al 2024 was studied within a classical thermodynamics framework. From the thermomechanical

formulation, fracture fatigue entropy (FFE) was estimated based on temperature measurements (where emissivity uncertainty is shown to have a small influence on the FFE estimation). Estimation of the FFE from a mechanical empirical model was also preformed. The various estimations seem to converge towards the fact that a constant FFE exists, where the Park and Nelson empirical model (corrected with the prefactor for mean stress) produces a value in accordance with the experimental determination procedure for well-chosen material parameters (UML parameters in this case). In this study, the influence of environment through convective and radiative parts are negligible, and in terms of exergy of plastic deformation, the results confirm the existence of a threshold. It can be noticed that, at $R = 0$, the primary short non stationary phase of tests produces a large amount of entropy and exergy due to the initial work hardening of the material. During the second longer stationary phase, the level of generated entropy and exergy stabilises until failure, indicating a quasi linear evolution of the damage.

Further tests would be appropriate to verify the independence of the testing parameter in a broader range of loadings and frequencies. Also, new tests will be conducted in specific environments where temperature, pressure or chemical potential can vary, in which the use of the exergy of plastic deformation may become the quantity to be studied replacing the fracture fatigue entropy.

Appendix A. Heat transfer coefficient estimation

Appendix A.1. Dimensionless numbers

The specimen is considered as a vertical plate being submitted to natural convection of air. To estimate heat transferred by convection, we need to estimate the convective heat transfer coefficient. This coefficient is related to the Nusselt number expressed as:

$$Nu = \frac{h_{conv} L_c}{\lambda_F} \tag{A.1}$$

In natural convection the dimensionless numbers of interest are the Prandtl number and the Grashof number (their product being the Rayleigh number) expressed as:

$$Ra = GrPr = \frac{g\beta_c \left(T_m - T_0\right) L^3}{\nu_{FT}\nu_{Fh}} \tag{A.2}$$

Thermophysical properties of air are evaluated at the film temperature, i.e. using a mean temperature taken between the vertical surface temperature of the specimen and the air temperature calculated from the empirical formulas in [77]. The estimation of the Nusselt number (and thus h_{conv}) is possible using the natural convection correlations on the Rayleigh number from the literature.

Appendix A.2. Correlations

Several correlations (equations (A.3),(A.4),(A.5) from [32] and equation (A.6) from [78]) exist for vertical plates submitted to natural convection leading to very close results for the convective heat transfer coefficient. The mean estimation (using an average on all the correlations) obtained for the convective heat transfer coefficient for each tests is plotted in figure A.9.

$$Nu = \left(0.825 + \frac{0.387\, Ra^{1/6}}{\left[1 + \left(\frac{0.492}{Pr} \right)^{9/16} \right]^{8/27}} \right)^2 \tag{A.3}$$

$$Nu = A\,(GrPr)^{1/4} \qquad A^4 = \frac{Pr}{2.43478 + 4.884\, Pr^{1/2} + 4.95283 Pr} \tag{A.4}$$

$$Nu = 0.667 \left(\frac{Pr}{0.952 + Pr} \right)^{1/4} Ra^{1/4} \tag{A.5}$$

$$Nu = 0.59 Ra^{1/4} \qquad 10^4 < Ra < 10^9 \qquad\qquad Nu = 0.13 Ra^{1/3} \qquad 10^9 < Ra < 10^{13} \tag{A.6}$$

We have here considered that our specimen was smooth, in the case of a rough surface, other correlations have to be used [79]. In addition, the former correlations are valid for specimens which are not moving. In our case, the loading implies a slight displacement which has to be studied.

Appendix A.3. Correlations validity

Since the fluid (air) is viscous its velocity is imposed by the specimen (no slip condition). To see if the velocity is imposed by the specimen cycling or through a density gradient (temperature gradient of the fluid), the two

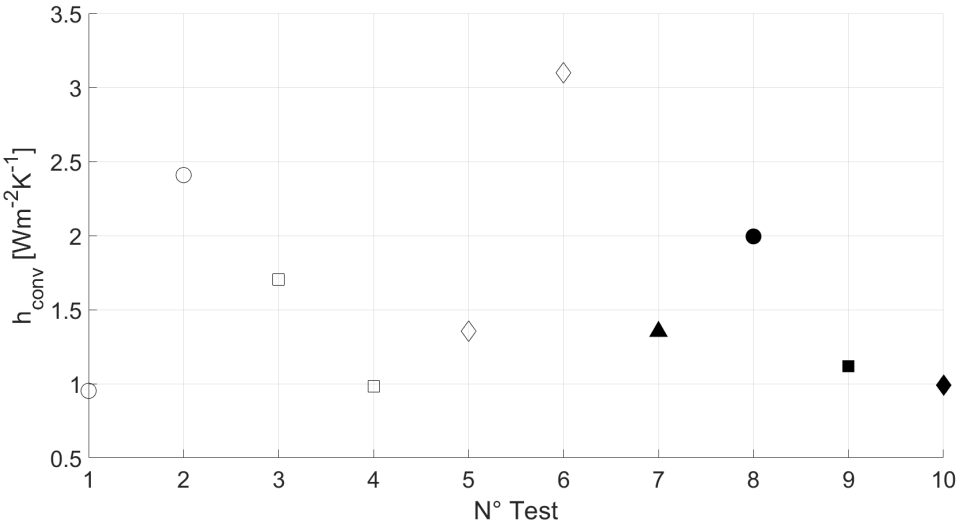

Figure A.9: Mean convective coefficient obtained from the calculation of the different Nusselt numbers given in equations (A.3) to (A.6) - Loads : △ : 410 MPa - ○ : 430 MPa - □ : 450 MPa - ◇ : 470 MPa ; Frequencies : Unfilled markers : 5 Hz - Filled markers : 10 Hz

components can be compared using the Richardson number (ratio of Grashof number to the squared Reynolds number) :

$$Ri = \frac{Gr}{Re^2} = \frac{g\beta_c \left(T_p - T_0\right) L}{v^2} \tag{A.7}$$

An order of magnitude of the velocity imposed by the specimen can be obtained considering that the velocity is near the velocity of the specimen in the elastic loading regime. Using table.1 and table.2, and the fact that the loading varies from 0 to maximal amplitude during the time $(1/2f)$ where f is the loading frequency, the worst case scenario (12 kN - 10 Hz) gives the mean velocity as :

$$v = \frac{\Delta l}{\Delta t} \approx \left(\frac{\Delta \sigma}{E_y}\right) \frac{L}{\Delta t} = 6.2 \times 10^{-3}\, ms^{-1} \tag{A.8}$$

The Richardson number is then approximately (taking $T_m - T_0$=1K):

$$Ri = \frac{9.81 \times (1/293.15) \times 1 \times 5.7 \times 10^{-2}}{(6.2 \times 10^{-3})^2} \approx 50 \tag{A.9}$$

We see here that the fluid flow is driven by the natural convection, and the velocity being small, the correlations for vertical planes are sufficient.

Appendix B. Emissivity error influence

When studying a particular range of wavelength $[\lambda_1, \lambda_2]$, one can perform the irradiance integration considering fractions of emitted power [80]:

$$\int_{\lambda_1}^{\lambda_2} L_\lambda d\lambda = [f(\lambda_2 T) - f(\lambda_1 T)]\varsigma T^4 \tag{B.1}$$

With :

$$f(\lambda T) = \frac{15}{\pi^4}\sum_{m=1}^{\infty}\frac{e^{m\xi}}{m^4}\left(6 + 6(m\xi) + 3(m\xi)^2 + (m\xi)^3\right) \qquad \xi = \frac{h_p c_l}{k_b \lambda T} \tag{B.2}$$

The comparison between black body and real body radiation is defined by the emission factor (ε) through a ratio between the black body irradiance and the real body irradiance (in the same conditions):

$$\varepsilon_\lambda(\lambda, T, \theta) = \frac{L_\lambda(\lambda, T, \theta)}{L^0_\lambda(\lambda, T)} \tag{B.3}$$

This factor is comprised between 0 and 1, and depends on the wavelength, temperature, emission angle, the material under study, its surface condition and optical parameters. From this factor, one can evaluate the irradiance temperature T_λ which is the temperature of a body if it was a black body. In the case of a range of wavelength, we have:

$$\int_\lambda L_\lambda(T) = \int_\lambda \varepsilon_\lambda L^0_\lambda(T) = \int_\lambda L^0_\lambda(T_\lambda) \tag{B.4}$$

In our case, we have hypothesised the value of the emissivity of our painted specimen being equal to 0.95 (experiments reveal that 0.95 is admissible for our conditions [81]). Recalling that the wavelength range is $\lambda \in [7.5 - 13]\,\mu m$, we can analyse the error committed on the temperature measurement if the emissivity was 0.9 or 0.85. Numerical calculation permits to estimate that for $\varepsilon = 0.9$ and $\varepsilon = 0.85$, the temperature has to be incremented by 3K and 6K respectively. This shift in the measured temperature does not imply many changes, indeed, the first method requiring a parabolic fit does not need the

intercept. In the convection part and in the estimation based on the exponential fit, environment temperature and material temperature are shifted thus temperature difference does not change. Finally, the only part changing is the radiative part, where the radiative equivalent transfer coefficient becomes (using Pascal's triangle):

$$h'_{rad} = 4(\varepsilon - c_1)\varsigma(T_0 + c_2)^3 \tag{B.5}$$

$$h'_{rad} = \underbrace{4\varepsilon\varsigma T_0^3}_{h_{rad}} + \left[(3T_0^2 \times c_2) + (3T_0 \times c_2^2) + c_2^3\right] - 4c_1\varsigma(T_0 + c_2)^3 \tag{B.6}$$

With: $T_0 \approx 18.7°C$, $h_0 \approx 5.36\, Wm^{-2}K^{-1}$ and $c_1 = \{0.05; 0.1\}$ and $c_2 = \{3; 6\}$. The calculation of the corrected radiative equivalent transfer coefficient implies $h'_{rad} = \{5.23; 5.10\}\, Wm^{-2}K^{-1}$ (less than 5% difference).

References

[1] A. Wohler, Uber die Festigkeitsversuche mit Eisen und Stahl, 1870.

[2] L. F. Coffin, A note on low cycle fatigue laws, Journal of Materials 6 (2) (1971) 388 – 402.

[3] S. S. Manson, Interpretive report on cumulative fatigue damage in the law cycle range, Welding Journal Research 43 (1964) 344 – 352.

[4] S. S. Manson, Fatigue : A complex subject - some simple approximations, Experimental Mechanics 5 (1964) 193 – 226.

[5] M. A. Miner, Cumulative damage in fatigue, Journal of Applied Mechanics 67 (1945) 159 – 164.

[6] J. Morrow, Cyclic plastic strain energy and fatigue of metals, ASTM STP 378 (1965) 45 – 87.

[7] G. R. Halford, The energy required for fatigue, Journal of Materials 1 (1966) 3 – 18.

[8] J. Park, D. Nelson, Evaluation of an energy-based approach and a critical plane approach for predicting constant amplitude multiaxial fatigue life, International Journal of Fatigue 22 (1) (2000) 23 – 39. doi:http://dx.doi.org/10.1016/S0142-1123(99)00111-5.
URL http://www.sciencedirect.com/science/article/pii/S0142112399001115

[9] J.-H. Park, J.-H. Song, Detailed evaluation of methods for estimation of fatigue properties, International Journal of Fatigue 17 (5) (1995) 365 – 373. doi:http://dx.doi.org/10.1016/0142-1123(95)99737-U.
URL http://www.sciencedirect.com/science/article/pii/014211239599737U

[10] A. Fatemi, A. Plaseied, A. Khosrovaneh, D. Tanner, Application of bi-linear loglog sn model to strain-controlled fatigue data of aluminum alloys and its effect on life predictions, International Journal of Fatigue 27 (9) (2005) 1040 – 1050. doi:http://dx.doi.org/10.1016/j.ijfatigue.2005.03.003.
URL http://www.sciencedirect.com/science/article/pii/S0142112305000770

[11] Q. Guo, X. Guo, J. Fan, R. Syed, C. Wu, An energy method for rapid evaluation of high-cycle fatigue parameters based on intrinsic dissipation, International Journal of Fatigue 80 (2015) 136 – 144. doi:http://dx.doi.org/10.1016/j.ijfatigue.2015.04.016.
URL http://www.sciencedirect.com/science/article/pii/S0142112315001322

[12] G. Meneghetti, M. Ricotta, The use of the specific heat loss to analyse the low- and high-cycle fatigue behaviour of plain and notched specimens made of a stainless steel, Engineering Fracture Mechanics 81 (2012) 2 – 16. doi:http://dx.doi.org/10.1016/j.engfracmech.2011.06.010.
URL http://www.sciencedirect.com/science/article/pii/S0013794411002347

[13] F. Maquin, F. Pierron, Heat dissipation measurements in low stress cyclic loading of metallic materials: From internal friction to micro-plasticity, Mechanics of Materials 41 (8) (2009) 928 – 942. doi:https://doi.org/10.1016/j.mechmat.2009.03.003.
URL http://www.sciencedirect.com/science/article/pii/S0167663609000696

[14] A. Kahirdeh, M. Khonsari, Energy dissipation in the course of the fatigue degradation: Mathematical derivation and experimental quantification, International Journal of Solids and Structures 77 (2015) 74 – 85. doi:http://dx.doi.org/10.1016/j.ijsolstr.2015.06.032.
URL http://www.sciencedirect.com/science/article/pii/S0020768315002966

[15] M. Bryant, M. Khonsari, F. Ling, On the thermodynamics of degradation, Proceedings of the Royal Society of London A: Mathematical, Physical and Engineering Sciences 464 (2096) (2008) 2001–2014. arXiv:http://rspa.royalsocietypublishing.org/content/464/2096/2001.full.pdf, doi:10.1098/rspa.2007.0371.
URL http://rspa.royalsocietypublishing.org/content/464/2096/2001

[16] K. L. Doelling, F. F. Ling, M. D. Bryant, B. P. Heilman, An experimental study of the correlation between wear and entropy flow in machinery components, Journal of Applied Physics 88 (5) (2000) 2999–3003.

arXiv:https://doi.org/10.1063/1.1287778, doi:10.1063/1.1287778.
URL https://doi.org/10.1063/1.1287778

[17] M. Amiri, M. Naderi, M. Khonsari, An experimental approach to evaluate the critical damage, International Journal of Damage Mechanics 20 (1) (2011) 89–112. arXiv:https://doi.org/10.1177/1056789509343082, doi:10.1177/1056789509343082.
URL https://doi.org/10.1177/1056789509343082

[18] C. Basaran, C.-Y. Yan, A Thermodynamic Framework for Damage Mechanics of Solder Joints, Journal of Electronic Packaging 120 (4) (1998) 379–384. arXiv:https://asmedigitalcollection.asme.org/electronicpackaging/article-pdf/120/4/379/4664209/379_1.pdf, doi:10.1115/1.2792650.
URL https://doi.org/10.1115/1.2792650

[19] T. C. Chu, W. F. Ranson, M. A. Sutton, Applications of digital-image-correlation techniques to experimental mechanics, Experimental Mechanics 25 (3) (1985) 232–244. doi:10.1007/BF02325092.
URL https://doi.org/10.1007/BF02325092

[20] J. D. Carroll, W. Abuzaid, J. Lambros, H. Sehitoglu, High resolution digital image correlation measurements of strain accumulation in fatigue crack growth, International Journal of Fatigue 57 (2013) 140 – 150, fatigue and Microstructure: A special issue on recent advances. doi:https://doi.org/10.1016/j.ijfatigue.2012.06.010.
URL http://www.sciencedirect.com/science/article/pii/S0142112312002113

[21] A. Kahirdeh, C. Sauerbrunn, H. Yun, M. Modarres, A parametric approach to acoustic entropy estimation for assessment of fatigue damage, International Journal of Fatigue 100 (2017) 229 – 237. doi:https://doi.org/10.1016/j.ijfatigue.2017.03.019.
URL http://www.sciencedirect.com/science/article/pii/S0142112317301159

[22] C. M. Sauerbrunn, A. Kahirdeh, H. Yun, M. Modarres, Damage assessment using information entropy of individual acoustic emission waveforms during cyclic fatigue loading, Applied Sciences 7 (6).

doi:10.3390/app7060562.
URL https://www.mdpi.com/2076-3417/7/6/562

[23] A. Keshtgar, C. M. Sauerbrunn, M. Modarres, Structural reliability prediction using acoustic emission-based modeling of fatigue crack growth, Applied Sciences 8 (8). doi:10.3390/app8081225.
URL https://www.mdpi.com/2076-3417/8/8/1225

[24] G. Fargione, A. Geraci, G. L. Rosa, A. Risitano, Rapid determination of the fatigue curve by the thermographic method, International Journal of Fatigue 24 (1) (2002) 11 – 19. doi:http://dx.doi.org/10.1016/S0142-1123(01)00107-4.
URL http://www.sciencedirect.com/science/article/pii/S0142112301001074

[25] G. La Rosa, A. Risitano, Thermographic methodology for rapid determination of the fatigue limit of materials and mechanical components, International Journal of Fatigue 22 (1) (2000) 65 – 73. doi:http://dx.doi.org/10.1016/S0142-1123(99)00088-2.
URL http://www.sciencedirect.com/science/article/pii/S0142112399000882

[26] J. Fan, X. Guo, C. Wu, A new application of the infrared thermography for fatigue evaluation and damage assessment, International Journal of Fatigue 44 (2012) 1 – 7. doi:https://doi.org/10.1016/j.ijfatigue.2012.06.003.
URL http://www.sciencedirect.com/science/article/pii/S0142112312002046

[27] A. Wong, G. Kirby, A hybrid numerical/experimental technique for determining the heat dissipated during low cycle fatigue, Engineering Fracture Mechanics 37 (3) (1990) 493 – 504. doi:https://doi.org/10.1016/0013-7944(90)90375-Q.
URL http://www.sciencedirect.com/science/article/pii/001379449090375Q

[28] V. Crupi, An unifying approach to assess the structural strength, International Journal of Fatigue 30 (7) (2008) 1150 – 1159. doi:https://doi.org/10.1016/j.ijfatigue.2007.09.007.

URL http://www.sciencedirect.com/science/article/pii/S0142112307002721

[29] L. Jiang, H. Wang, P. Liaw, C. Brooks, D. Klarstrom, Temperature evolution during low-cycle fatigue of ultimet alloy: experiment and modeling, Mechanics of Materials 36 (1) (2004) 73 – 84, fatigue of Advanced Materials. doi:https://doi.org/10.1016/S0167-6636(03)00032-2.
URL http://www.sciencedirect.com/science/article/pii/S0167663603000322

[30] M. Amiri, M. M. Khonsari, Rapid determination of fatigue failure based on temperature evolution: Fully reversed bending load, International Journal of Fatigue 32 (2) (2010) 382 – 389. doi:http://dx.doi.org/10.1016/j.ijfatigue.2009.07.015.
URL http://www.sciencedirect.com/science/article/pii/S0142112309002382

[31] M. Amiri, M. Khonsari, Life prediction of metals undergoing fatigue load based on temperature evolution, Materials Science and Engineering: A 527 (6) (2010) 1555 – 1559. doi:http://dx.doi.org/10.1016/j.msea.2009.10.025.
URL http://www.sciencedirect.com/science/article/pii/S092150930901154X

[32] G. Meneghetti, Analysis of the fatigue strength of a stainless steel based on the energy dissipation, International Journal of Fatigue 29 (2007) 81 – 94.

[33] A. Chrysochoos, H. Louche, An infrared image processing to analyse the calorific effects accompanying strain localisation, International Journal of Engineering Science 38 (16) (2000) 1759 – 1788. doi:http://dx.doi.org/10.1016/S0020-7225(00)00002-1.
URL http://www.sciencedirect.com/science/article/pii/S0020722500000021

[34] G. Meneghetti, M. Ricotta, B. Atzori, A synthesis of the push-pull fatigue behaviour of plain and notched stainless steel specimens by using the specific heat loss, Fatigue & Fracture of Engineering Materials & Structures 36 (12) (2013) 1306–1322. arXiv:https://onlinelibrary.wiley.com/doi/pdf/10.1111/ffe.12071,

doi:10.1111/ffe.12071.
URL https://onlinelibrary.wiley.com/doi/abs/10.1111/ffe.12071

[35] A. Risitano, G. Risitano, Cumulative damage evaluation of steel using infrared thermography, Theoretical and Applied Fracture Mechanics 54 (2) (2010) 82 – 90. doi:https://doi.org/10.1016/j.tafmec.2010.10.002.
URL http://www.sciencedirect.com/science/article/pii/S0167844210000698

[36] A. Risitano, G. Risitano, Cumulative damage evaluation in multiple cycle fatigue tests taking into account energy parameters, International Journal of Fatigue 48 (2013) 214 – 222. doi:https://doi.org/10.1016/j.ijfatigue.2012.10.020.
URL http://www.sciencedirect.com/science/article/pii/S0142112312003210

[37] Y. F. Ital'yantsev, Thermodynamic state of deformed solids. report 1. determination of local functions of state, Strength of Materials 16 (2) (1984) 238–241. doi:10.1007/BF01530067.
URL http://dx.doi.org/10.1007/BF01530067

[38] Y. F. Ital'yantsev, Thermodynamic state of deformed solids. report 2. entropy failure criteria and their application for simple tensile loading problems, Strength of Materials 16 (2) (1984) 242–247. doi:10.1007/BF01530068.
URL http://dx.doi.org/10.1007/BF01530068

[39] P. Whaley, Y. Pao, K. Lin, Numerical simulation of material fatigue by a thermodynamic approach. arXiv:https://arc.aiaa.org/doi/pdf/10.2514/6.1983-977, doi:10.2514/6.1983-977.
URL https://arc.aiaa.org/doi/abs/10.2514/6.1983-977

[40] C. Basaran, S. Nie, An irreversible thermodynamics theory for damage mechanics of solids, International Journal of Damage Mechanics 13 (3) (2004) 205–223. arXiv:http://ijd.sagepub.com/content/13/3/205.full.pdf+html, doi:10.1177/1056789504041058.
URL http://ijd.sagepub.com/content/13/3/205.abstract

[41] M. Amiri, M. Modarres, An entropy-based damage characterization, Entropy 16 (12) (2014) 6434. doi:10.3390/e16126434.
URL http://www.mdpi.com/1099-4300/16/12/6434

[42] M. Naderi, M. Amiri, M. M. Khonsari, On the thermodynamic entropy of fatigue fracture, Proceedings of the Royal Society of London A: Mathematical, Physical and Engineering Sciences 466 (2114) (2010) 423–438. doi:10.1098/rspa.2009.0348.
URL http://rspa.royalsocietypublishing.org/content/466/2114/423

[43] M. Amiri, M. M. Khonsari, On the role of entropy generation in processes involving fatigue, Entropy 14 (1) (2012) 24. doi:10.3390/e14010024.
URL http://www.mdpi.com/1099-4300/14/1/24

[44] M. Khonsari, M. Amiri, Introduction to thermodynamics of Mechanical Fatigue, CRC press, Boca Raton, 2017.

[45] M. Liakat, M. Khonsari, Entropic characterization of metal fatigue with stress concentration, International Journal of Fatigue 70 (2015) 223 – 234. doi:http://dx.doi.org/10.1016/j.ijfatigue.2014.09.014.
URL http://www.sciencedirect.com/science/article/pii/S0142112314002424

[46] M. Liakat, M. Khonsari, On the anelasticity and fatigue fracture entropy in high-cycle metal fatigue, Materials and Design 82 (2015) 18 – 27. doi:http://dx.doi.org/10.1016/j.matdes.2015.04.034.
URL http://www.sciencedirect.com/science/article/pii/S0261306915002162

[47] M. Naderi, M. Khonsari, Real-time fatigue life monitoring based on thermodynamic entropy, Structural Health Monitoring 10 (2) (2011) 189–197. arXiv:https://doi.org/10.1177/1475921710373295, doi:10.1177/1475921710373295.
URL https://doi.org/10.1177/1475921710373295

[48] M. Naderi, M. Khonsari, An experimental approach to low-cycle fatigue damage based on thermodynamic entropy, International Journal of Solids and Structures 47 (6) (2010) 875 – 880.

doi:http://dx.doi.org/10.1016/j.ijsolstr.2009.12.005.
URL http://www.sciencedirect.com/science/article/pii/S0020768309004703

[49] M. Naderi, M. Khonsari, A thermodynamic approach to fatigue damage accumulation under variable loading, Materials Science and Engineering: A 527 (23) (2010) 6133 – 6139. doi:http://dx.doi.org/10.1016/j.msea.2010.05.018.
URL http://www.sciencedirect.com/science/article/pii/S0921509310005307

[50] V. L. Ontiveros, M. Modarres, M. Amiri, Estimation of reliability of structures subject to fatigue loading using plastic strain energy and thermodynamic entropy generation, Proceedings of the Institution of Mechanical Engineers, Part O: Journal of Risk and Reliability arXiv:http://pio.sagepub.com/content/early/2015/02/27/1748006X15574143.full.pdf+html, doi:10.1177/1748006X15574143.
URL http://pio.sagepub.com/content/early/2015/02/27/1748006X15574143.abstract

[51] V. Ontiveros, M. Amiri, A. Kahirdeh, M. Modarres, Thermodynamic entropy generation in the course of the fatigue crack initiation, Fatigue & Fracture of Engineering Materials & Structures 40 (3) (2017) 423–434. arXiv:https://onlinelibrary.wiley.com/doi/pdf/10.1111/ffe.12506, doi:10.1111/ffe.12506.
URL https://onlinelibrary.wiley.com/doi/abs/10.1111/ffe.12506

[52] A. Imanian, M. Modarres, A thermodynamic entropy approach to reliability assessment with applications to corrosion fatigue, Entropy 17 (10) (2015) 6995–7020. doi:10.3390/e17106995.
URL https://www.mdpi.com/1099-4300/17/10/6995

[53] J. Wang, Y. Yao, An entropy based low-cycle fatigue life prediction model for solder materials, Entropy 19 (10). doi:10.3390/e19100503.
URL https://www.mdpi.com/1099-4300/19/10/503

[54] H. Yun, M. Modarres, Measures of entropy to characterize fatigue damage in metallic materials, Entropy 21 (8). doi:10.3390/e21080804.
URL https://www.mdpi.com/1099-4300/21/8/804

[55] J. A. Osara, M. D. Bryant, Thermodynamics of fatigue: Degradation-entropy generation methodology for system and process characterization and failure analysis, Entropy 21 (7). doi:10.3390/e21070685.
URL https://www.mdpi.com/1099-4300/21/7/685

[56] Y.-J. Sun, L.-S. Hu, Assessment of Low Cycle Fatigue Life of Steam Turbine Rotor Based on a Thermodynamic Approach, Journal of Engineering for Gas Turbines and Power 134 (6), 064504. arXiv:https://asmedigitalcollection.asme.org/gasturbinespower/article-pdf/134/6/064504/4792196/064504_1.pdf, doi:10.1115/1.4006004.
URL https://doi.org/10.1115/1.4006004

[57] S. F. Karimian, H. A. Bruck, M. Modarres, Thermodynamic entropy to detect fatigue crack initiation using digital image correlation, and effect of overload spectrums, International Journal of Fatigue 129 (2019) 105256. doi:https://doi.org/10.1016/j.ijfatigue.2019.105256.
URL http://www.sciencedirect.com/science/article/pii/S0142112319303603

[58] H. Salimi, M. Pourgol-Mohammad, M. Yazdani, Metal fatigue assessment based on temperature evolution and thermodynamic entropy generation, International Journal of Fatigue 127 (2019) 403 – 416. doi:https://doi.org/10.1016/j.ijfatigue.2019.06.022.
URL http://www.sciencedirect.com/science/article/pii/S014211231930252X

[59] M. Liakat, M. Khonsari, An experimental approach to estimate damage and remaining life of metals under uniaxial fatigue loading, Materials and Design 57 (2014) 289 – 297. doi:http://dx.doi.org/10.1016/j.matdes.2013.12.027.
URL http://www.sciencedirect.com/science/article/pii/S0261306913011606

[60] M. Liakat, M. Khonsari, Rapid estimation of fatigue entropy and toughness in metals, Materials and Design (1980-2015) 62 (2014) 149 – 157. doi:http://dx.doi.org/10.1016/j.matdes.2014.04.086.
URL http://www.sciencedirect.com/science/article/pii/S0261306914003616

[61] M. Mehdizadeh, M. Khonsari, On the role of internal friction in low-and high-cycle fatigue, International Journal of Fatigue 114 (2018) 159 – 166. doi:https://doi.org/10.1016/j.ijfatigue.2018.05.007.
URL http://www.sciencedirect.com/science/article/pii/S0142112318301786

[62] M. Mehdizadeh, M. Khonsari, On the application of fracture fatigue entropy to variable frequency and loading amplitude, Theoretical and Applied Fracture Mechanics 98 (2018) 30 – 37. doi:https://doi.org/10.1016/j.tafmec.2018.09.005.
URL http://www.sciencedirect.com/science/article/pii/S016784421830329X

[63] J. Lemaitre, J. Chaboche, Mechanics of Solid Materials, Cambridge University press, Cambridge UK, 1990.

[64] A. Bäumel, T. Seeger, Materials data for cyclic loading, Elsevier Science Publishers, 1990.

[65] M. Meggiolaro, J. Castro, Statistical evaluation of strain-life fatigue crack initiation predictions, International Journal of Fatigue 26 (5) (2004) 463 – 476. doi:http://dx.doi.org/10.1016/j.ijfatigue.2003.10.003.
URL http://www.sciencedirect.com/science/article/pii/S0142112303002469

[66] A. Lipski, S. Mroziński, Approximate determination of a strain-controlled fatigue life curve for aluminum alloy sheets for aircraft structures, International Journal of Fatigue 39 (2012) 2 – 7, physical and phenomenological approaches to fatigue damage. doi:http://dx.doi.org/10.1016/j.ijfatigue.2011.08.007.
URL http://www.sciencedirect.com/science/article/pii/S0142112311002064

[67] A. Ince, G. Glinka, A modification of morrow and smithwatsontopper mean stress correction models, Fatigue & Fracture of Engineering Materials & Structures 34 (11) 854–867. doi:10.1111/j.1460-2695.2011.01577.x.
URL https://onlinelibrary.wiley.com/doi/abs/10.1111/j.1460-2695.2011.01577.x

[68] N. E. Dowling, Mean stress effects in stress-life and strain-life fatigue, in: SAE Technical Paper, SAE International, 2004. doi:10.4271/2004-01-2227.
URL https://doi.org/10.4271/2004-01-2227

[69] T. Boulanger, A. Chrysochoos, C. Mabru, A. Galtier, Calorimetric analysis of dissipative and thermoelastic effects associated with the fatigue behavior of steels, International Journal of Fatigue 26 (3) (2004) 221 – 229. doi:http://dx.doi.org/10.1016/S0142-1123(03)00171-3.
URL http://www.sciencedirect.com/science/article/pii/S0142112303001713

[70] A. Blanche, A. Chrysochoos, N. Ranc, V. Favier, Dissipation assessments during dynamic very high cycle fatigue tests, Experimental Mechanics 55 (4) (2015) 699–709. doi:10.1007/s11340-014-9857-3.
URL http://dx.doi.org/10.1007/s11340-014-9857-3

[71] A. Chrysochoos, J.-C. Chezeaux, H. Caumon, Analyse thermomécanique des lois de comportement par thermographie infrarouge, Rev. Phys. Appl. (Paris) 24 (2) (1989) 215–225. doi:10.1051/rphysap:01989002402021500.
URL http://dx.doi.org/10.1051/rphysap:01989002402021500

[72] A. Chrysochoos, R. Peyroux, Analyse expérimentale et modélisation numérique des couplages thermomécaniques dans les matériaux solides, Revue Générale de Thermique 37 (7) (1998) 582 – 606. doi:http://dx.doi.org/10.1016/S0035-3159(98)80036-6.
URL http://www.sciencedirect.com/science/article/pii/S0035315998800366

[73] E. M. Pellegrino, E. Ghibaudi, L. Cerruti, Clausius disgregation: A conceptual relic that sheds light on the second law, Entropy 17 (7) (2015) 4500–4518. doi:10.3390/e17074500.
URL http://www.mdpi.com/1099-4300/17/7/4500

[74] M. Gouy, Sur l'énergie utilisable, Journal de physique théorique et appliquée 8 (1) (1889) 501 – 518.

[75] J. Keenan, Availability and irreversibility in thermodynamics, British Journal of Applied Physics 2 (7) (1951) 183 – 192.

[76] P. Ribeiro, D. Queiros-Condé, L. Grosu, L. Gallimard, An exergetic approach for materials fatigue, International Journal of Exergy 22 (3) (2017) 235–249. doi:10.1504/IJEX.2017.083172.
URL https://www.inderscienceonline.com/doi/abs/10.1504/IJEX.2017.08317

[77] J. C. Dixon, Appendix B: Properties of Air, Wiley-Blackwell, 2007, pp. 375–378. doi:10.1002/9780470516430.app2.
URL https://onlinelibrary.wiley.com/doi/abs/10.1002/9780470516430.app2

[78] B. Eyglunent, Manuel de thermique théorie et pratique (2e éd.), Hermès, 1997.

[79] M. Ashjaee, M. Amiri, J. Rostami, A correlation for free convection heat transfer from vertical wavy surfaces, Heat and Mass Transfer 44 (1) (2007) 101–111. doi:10.1007/s00231-006-0221-8.
URL http://dx.doi.org/10.1007/s00231-006-0221-8

[80] M. F. Modest, Radiative heat transfer, 3rd Edition, Elsevier, 2013.

[81] S. M. Baumann, Direct emissivity measurements of painted metals for improved temperature estimation during laser damage testing, Ph.D. thesis, Air Force Institute of Technology (2014).